IOPscience iopscience.iop.org

Home Search Collections Journals About Contact us My IOPscience

Flexible graphene–PZT ferroelectric nonvolatile memory

This content has been downloaded from IOPscience. Please scroll down to see the full text.

2013 Nanotechnology 24 475202

(http://iopscience.iop.org/0957-4484/24/47/475202)

View the table of contents for this issue, or go to the journal homepage for more

Download details:

IP Address: 165.132.45.198
This content was downloaded on 10/05/2016 at 08:54

Please note that terms and conditions apply.

Nanotechnology **24** (2013) 475202 (6pp) doi:10.1088/0957-4484/24/47/475202

Flexible graphene–PZT ferroelectric nonvolatile memory

Wonho Lee[1], Orhan Kahya[2,3], Chee Tat Toh[2,3], Barbaros Özyilmaz[2,3] and Jong-Hyun Ahn[1]

[1] School of Electrical and Electronic Engineering, Yonsei University, Seoul, 120-749, Korea
[2] Department of Physics, 2 Science Drive 3, National University of Singapore 117542, Singapore
[3] Graphene Research Centre, 6 Science Drive 2, National University of Singapore 117546, Singapore

E-mail: ahnj@yonsei.ac.kr

Received 13 August 2013, in final form 27 September 2013
Published 5 November 2013
Online at stacks.iop.org/Nano/24/475202

Abstract
We report the fabrication of a flexible graphene-based nonvolatile memory device using $Pb(Zr_{0.35}, Ti_{0.65})O_3$ (PZT) as the ferroelectric material. The graphene and PZT ferroelectric layers were deposited using chemical vapor deposition and sol–gel methods, respectively. Such PZT films show a high remnant polarization (P_r) of 30 μC cm^{-2} and a coercive voltage (V_c) of 3.5 V under a voltage loop over $\pm$11 V. The graphene–PZT ferroelectric nonvolatile memory on a plastic substrate displayed an on/off current ratio of 6.7, a memory window of 6 V and reliable operation. In addition, the device showed one order of magnitude lower operation voltage range than organic-based ferroelectric nonvolatile memory after removing the anti-ferroelectric behavior incorporating an electrolyte solution. The devices showed robust operation in bent states of bending radii up to 9 mm and in cycling tests of 200 times. The devices exhibited remarkable mechanical properties and were readily integrated with plastic substrates for the production of flexible circuits.

S Online supplementary data available from stacks.iop.org/Nano/24/475202/mmedia

(Some figures may appear in colour only in the online journal)

1. Introduction

The development of flexible memory devices is an essential step toward realizing flexible electronics for use in multi-functional systems such as displays, smart cards and sensor applications [1–3]. Ferroelectric field effect transistor (FeFET)-based memory devices have been extensively developed as nonvolatile memory devices. Poor mechanical properties present a significant hurdle to achieving flexible FeFET memory devices using conventional inorganic semiconductors and ferroelectric materials [4, 5]. Such issues may be overcome by using graphene-based FETs and organic ferroelectric materials such as poly(vinylidene fluoride-co-trifluoroethylene) [P(VDF-TrFE)]. It is reported that graphene grown by chemical vapor deposition (CVD) and P(VDF-TrFE) can hold up well under high strain of over 5% [6, 7]. Examples of flexible electronic devices such as nanogenerator and memory have been demonstrated by using such good mechanical property [8, 9]. However, the low polarizing performance and poor reliability of organic ferroelectrics relative to inorganic ferroelectrics limits the utility of these approaches in real device applications [10–12].

In this paper, we describe the preparation of flexible graphene-based FeFET memory arrays based on inorganic PZT ferroelectric thin ribbon structures. The PZT ferroelectric ribbons, which had been printed on a plastic substrate using transfer methods, exhibited good mechanical flexibility and great electrical performance [13, 14]. We also describe a method for overcoming the anti-ferroelectric effects of FeFET memory using electrolyte treatments. The graphene-based FeFET memory devices fabricated on inorganic ferroelectrics, as reported previously, tend to display unexpected reverse hysteresis loop behavior due to nonuniform charge induction and charge trapping at the interfaces between the channel and the ferroelectric layers. Such charge trapping effects seriously reduce the device performance [15, 16]. An electrolyte

 © 2013 IOP Publishing Ltd Printed in the UK & the USA

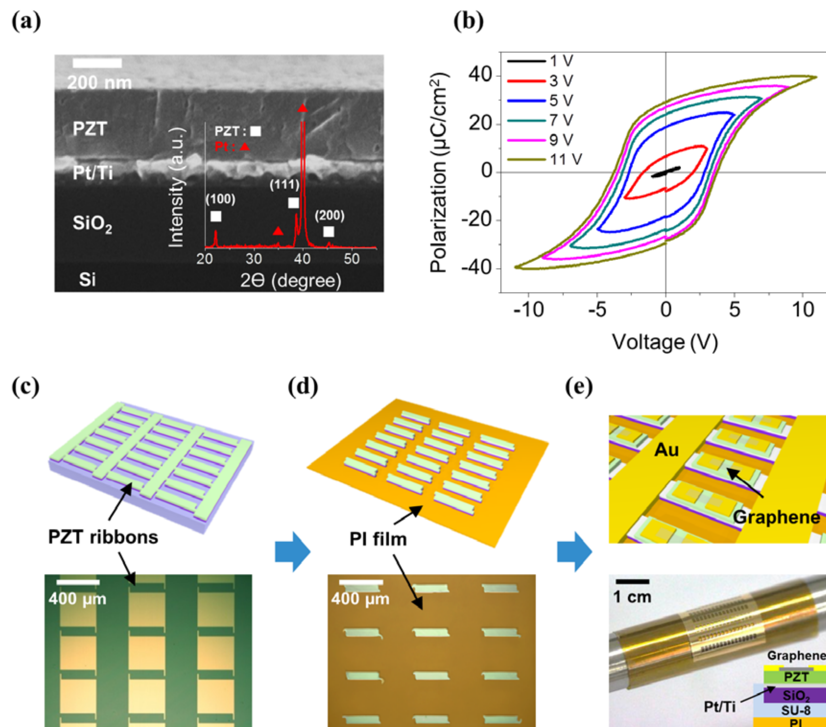

Figure 1. (a) Cross-sectional image of a PZT film formed on a Pt/Ti/SiO_2/Si wafer and characterized by scanning electron microscopy (SEM). The inset shows the XRD patterns of the PZT layer formed on a (111)-oriented Pt thin film by the sol–gel process. (b) Polarization versus voltage characteristics of the PZT film under different applied voltage loops. (c) Arrays of the PZT ribbons were defined using a wet etching process. (d) Well-arranged PZT ribbons on a PI substrate were transferred using a dry transfer method. (e) An illustration (top) and optical image of the fabricated flexible FeFET device on a PI substrate. The inset shows a schematic cross-sectional view of the device.

treatment was found to solve these effects, recovering the clockwise direction of the current hysteresis loop [17].

2. Experimental details

The PZT film was grown using a conventional sol–gel method which allows for an easy composition tuning process and yields a low residual stress. The fabrication process began with the preparation of a 0.4 M PZT solution using the precursors—lead acetate trihydrate ($Pb(CH_3CO_2)_2{\cdot}3H_2O$), zirconium n-propoxide ($Zr(C_3H_7O)_4$) and titanium-isopropoxide $Ti(C_3H_7O_3)$, and 2-methoxyethanol ($C_3H_8O_2$) as a solvent, with a 35/65 composition ratio of Zr/Ti. This process primarily forms a tetragonal-phase PZT layer featuring more effective ferroelectric properties than other phases [18]. The solution was spin-coated at 4000 rpm for 20 s repeatedly six times on a Pt (100 nm)/Ti (20 nm)/SiO_2 (300 nm)/Si wafer that promoted the crystallization of a perovskite PZT structure after each coating, followed by baking at 300 °C for 5 min [19]. The sample structure was subsequently annealed for 30 min at 650 °C to promote the crystallization. The structure and thickness of the multi-stacked layers (PZT (270 nm)/Pt (100 nm)/Ti (20 nm)/SiO_2 (300 nm)/Si) were characterized by scanning electron microscopy (SEM) and x-ray diffraction (XRD) methods. XRD indicated that PZT film was dominantly composed of (111)-orientation, although it included a small portion of (100)-oriented film which shows a little lower values of remnant polarization and coercive field than those of (111) (figure 1(a)). It is known that these mixed structures do not have a critical effect on the performance of the PZT films [20, 21]. The polarizing characteristics of the resulting PZT films were evaluated by measuring the polarization hysteresis loop response over various sweep voltages (1–11 V). A remnant polarization (P_r) of 30 μC cm^{-2} and a coercive voltage (V_c) of 3.5 V were determined under a voltage loop over ±11 V. These values are comparable with those of the crystalline PZT films produced through other methods, and also higher than those observed in organic ferroelectrics even at low operating voltages (see figure 1(b) and supplementary information available at stacks.iop.org/Nano/24/475202/mmedia). The crystallinity and polarizing properties of the PZT film were confirmed, and the structure was used in subsequent fabrication steps toward the preparation of flexible graphene-based FeFET memory devices.

Figures 1(c)–(e) show schematic illustrations of the steps involved in fabricating a flexible graphene-based FET memory device on a plastic substrate. First, the PZT films were used to form ribbon arrays connected through anchors prepared by photolithography. Wet etching with diluted HF was applied to remove unnecessary PZT regions (figure 1(c)). The Pt/Ti and SiO_2 layers were etched vertically and the bottom sacrificial silicon was laterally etched using inductively coupled plasma (ICP) etching techniques with SF_6 and CHF_3 gases to form free-standing ribbons. The PZT/Pt/Ti/SiO_2 ribbons were then lifted using

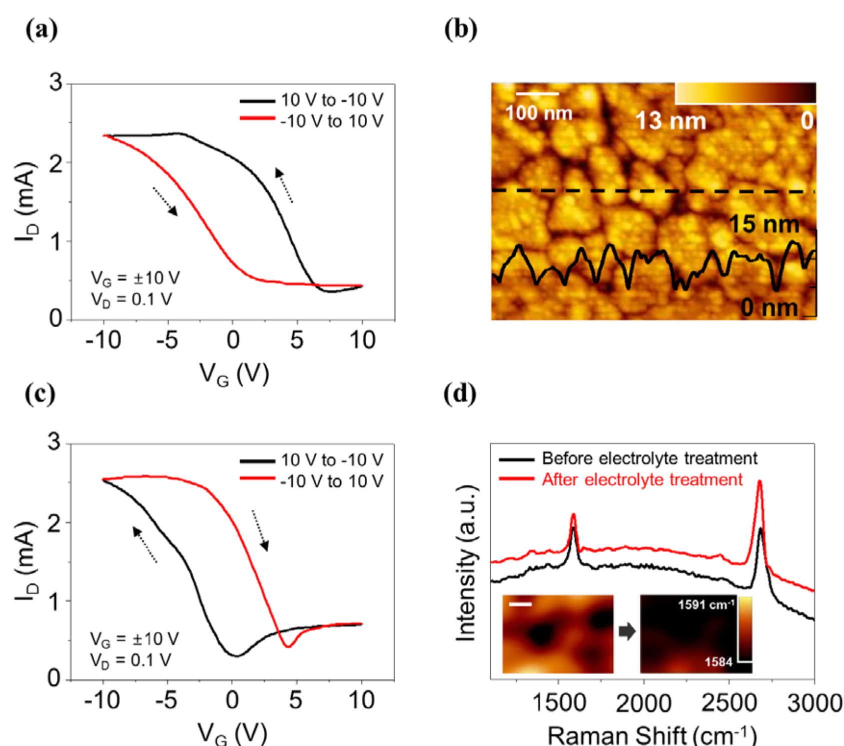

Figure 2. (a) I_D–V_G transfer characteristics of the as-fabricated graphene on PZT. (b) Atomic force microscopy (AFM) image of PZT surface and height profile (black solid line) of the PZT surface along the black dashed line. (c) I_D–V_G transfer characteristics of graphene on PZT, showing the changes in the loop direction after electrolyte treatment. (d) Raman spectra of a monolayer graphene film on PZT before and after electrolyte treatment. The inset images show the mapping of 'G' peaks corresponding to graphene on PZT before and after electrolyte treatment. (Scale bar: 2 μm.)

a polydimethylsiloxane (PDMS) stamp and were strongly attached onto a polyimide (PI) film (25 μm thick) using an adhesive epoxy layer (figure 1(d)). Cr/Au (3 nm/80 nm) electrodes were defined by photolithography and prepared using the lift-off method. Graphene grown by CVD methods was transferred and patterned onto the PZT ribbons to form an active channel layer. Finally, the fabrication of flexible graphene-based FeFET memory arrays mounted on a PI substrate were completed (figure 1(e)).

3. Results and discussion

As mentioned previously, the anti-ferroelectric properties of the channel surface states or the interfaces between the channel and inorganic ferroelectrics can produce a reverse current hysteresis loop in a memory device composed of graphene and PZT [15, 16]. The as-fabricated devices displayed a reverse current hysteresis loop, in contrast to the expected direction based on ferroelectricity in the I_D–V_G transfer characteristics (figure 2(a)). This unexpected result arose from the unstable surface and interface states of the PZT and graphene. The high roughness of the PZT surface disrupted the contact between the graphene and PZT layers to create weak polarizing interactions with the channel layer [22]. In addition, numerous grain boundaries and impurities were present and created trapped charges in the channel region due to the large channel area (10 μm × 80 μm) in comparison with 200 nm × 200 nm sized grains of PZT (figure 2(b)) [23]. A variety of factors may contribute to the ferroelectric field disturbance, including the presence of hydroxyl groups chemisorbed onto the surfaces of the PZT and graphene, or the dynamic dissociation and recombination of water molecules; therefore, the direction of the current hysteresis loop was reversed relative to the original direction [15, 24]. To overcome the anti-ferroelectric effects on the devices, we developed a method of using electrolytes to shift the Dirac voltage in a graphene FET toward 0 V by suppressing the charge trapping effects [25, 26]. Here, an electrolyte solution was sprayed on the top surface of the graphene/PZT/Pt structure. It was composed of 1-ethyl-3-methylimidazolium bis(tri-fluoromethylsulfonyl) imide ([EMIM][TFSI]), ($C_8H_{11}F_6N_3O_4S_2$) dissolved in methylene chloride (supplementary information available at stacks.iop.org/Nano/24/475202/mmedia) [27]. The surface covering was maintained over 24 h to be wet for the interface sufficiently. However, the electrolyte solution can easily make contact with the electrodes of the FET which results in a loss of ferroelectric function of the PZT and serious leakage of current. Therefore, the electrolyte solution was removed to prohibit connection between the solution and the electrodes. After the electrolyte solution was removed, the top surface of graphene was partially covered by the electrolyte solution (supplementary information available at stacks.iop.org/Nano/24/475202/mmedia). Electrolytes with

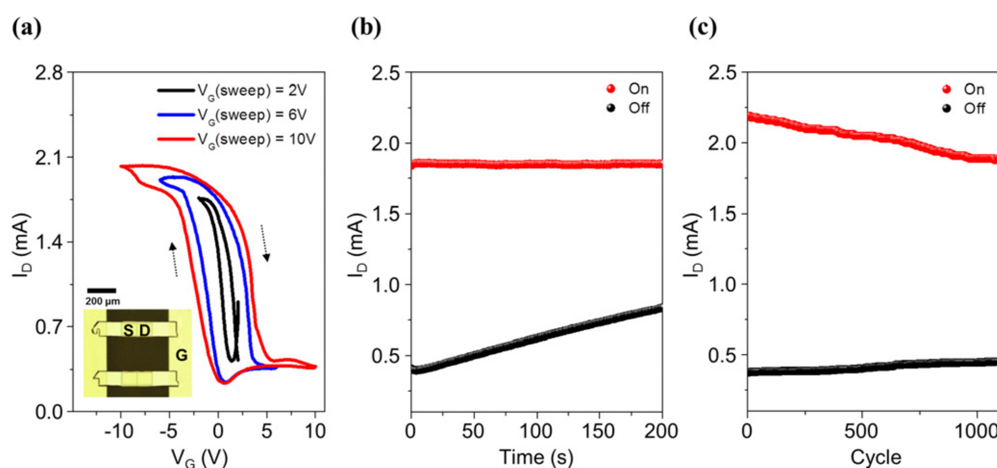

Figure 3. (a) I_D–V_G transfer characteristics of a flexible graphene FeFET on PZT with an electrolyte treatment under different applied voltage loops of 2, 6, 10 V at a drain voltage of 0.1 V. A channel length and a width are 10 μm and 80 μm, respectively. (b) Time retention properties of the graphene FeFET devices at a fixed drain voltage of 0.1 V. (c) Endurance test, in which the on and off currents were measured at a fixed drain voltage of 0.1 V over the working cycles.

heavy molecular weight of 391.31 g mol^{-1} cannot permeate through the normal defect site on the high quality graphene sheets [28, 29]. The electrolyte solution may be absorbed into the interfaces between graphene and PZT substrates through the structural defects of graphene such as edges, wrinkles and folded parts [30, 31]. Similarly, the solution can form thin layers beneath a graphene sheet and then fill the gap between the graphene and the highly rough surface of PZT. The high capacitance of the electrolytes compensated for the anti-ferroelectric effects and contributed to the effective ferroelectric polarization [32, 33]. The presence of the electrolytes reversed the counter-clockwise current hysteresis loop direction as a result of the increased ferroelectric properties, as shown in figure 2(c).

We characterized the effects of the electrolyte treatments on the graphene surface and interface chemistries using Raman spectroscopy. The positions of the 'G' and '2D' peaks corresponding to graphene on a substrate generally display a shift in the Raman spectrum that is distinct from the peak position in pristine graphene because of doping effect by the substrate [34, 35]. The graphene film transferred onto the PZT yielded 'G' and '2D' peak positions of 1589 and 2687 cm^{-1} (figure 2(d)). However, the peak positions were shifted to 1585 cm^{-1} and 2680 cm^{-1} from the initial positions, respectively after electrolyte treatments as visualized in the inset of figure 2(d)—the confocal mapping images of the 'G' peaks before and after electrolyte treatments. The intensity ratio I_{2D}/I_G increased from 1.62 to 2.41 following the electrolyte treatments. The peaks underwent a red shift and an increase in the I_{2D}/I_G ratio after electrolyte treatment, indicating that the factors contributing to p-type graphene doping, such as the charge trapping effects, were suppressed [36]. The electrolyte treatments enabled the preparation of both capacitor- and transistor-type ferroelectric memory devices based on PZT and graphene, which displayed ferroelectric properties (supplementary information available at stacks.iop.org/Nano/24/475202/mmedia).

Figure 3(a) shows the I_D–V_G transfer characteristics of the transistor fabricated with a channel length (L_C) of 10 μm and a channel width (W_C) of 80 μm for various sweep voltages at a fixed drain voltage of 0.1 V and the inset displays a top-view image of the devices, indicating source, drain and gate. The direction of the current hysteresis loop was found to be clockwise over the gate sweep ranges 2 to −2 V, 6 to −6 V, and 10 to −10 V, which indicates that the electrical properties of the device agreed with the ferroelectric characteristics of the PZT film in contrast to the previously reported tendency [15, 16]. The devices showed a small memory window of 6 V at a low operating voltage loop of ±10 V, which agreed well with the 2 × V_c value [37]. The on/off current ratio of the device was calculated to be 6.7, as the on current value of 1.79 mA at 0 V was divided by the off current value of 0.267 mA at V_G(sweep) = ±10 V.

One of the important properties of FeFET memory is memory retention. Figure 3(b) shows the retention properties of the devices, which were evaluated by measuring the on/off current value as a function of time after applying a writing and erasing pulse of ±10 V at a fixed drain voltage of 0.1 V. The on current value was preserved up to 200 s, whereas the off current value increased gradually up to 0.7 mA from 0.4 mA. Although the retention time of the device was shorter than reported values for other graphene-based FeFET memory devices, this is meaningful as a first demonstration of flexible FeFET memory devices based on graphene and PZT operated by the ferroelectric property. The retention characteristics could potentially be improved using methods for encapsulating the device and controlling the external conditions [24, 38]. The cycling characteristics are also important in that they can be used to evaluate the device stability over repetitive operations. The on/off currents were measured as a function of the cycling number of current–voltage loops, as displayed in figure 3(c). The on/off current was measured to be V_D = 0.1 V and the pre-applied voltage was fixed to ±10 V. Although the initial

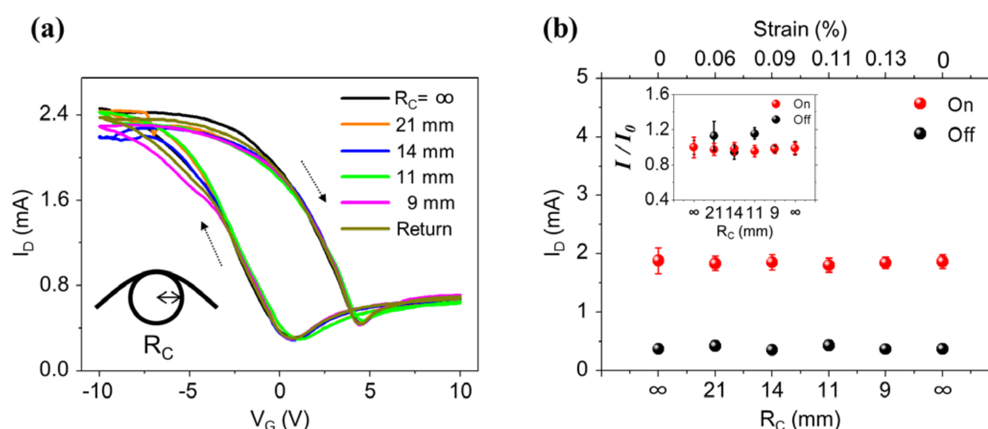

Figure 4. (a) Current–voltage characteristics of a graphene FeFET on PZT under bending conditions, with bending radii of ∞, 21, 14, 11, 9; also shown is the return at a drain voltage of 0.1 V. (b) Changes in the on/off current values at different bending radii (R_C) for a drain voltage of 0.1 V. The inset shows the normalized value of the change in the bending test.

on/off current values were 2.2 and 0.32 mA, the on current value decreased and the off current value increased slightly as the cycling number increased. Finally, the on and off current values shifted to 1.9 mA and 0.46 mA, respectively, and the ratio of the on/off current decreased to 3.5 (from 6.8) after 1000 cycles. The changes in the current value as a function of the *I–V* loop cycle resulted from the similar underlying factors that contributed to the shifts in the on and off current values during the retention test. The adsorption of impurities onto the graphene surfaces may have been responsible for these changes because the experiments were conducted under ambient conditions without an encapsulation layer [24, 38]. PZT layer degradation, which results from fatigue effects, could also have contributed to the on/off current changes during the cycling tests [39].

Our devices are distinguished from other inorganic-based FeFET memory devices by the device flexibility. The stability of the device performance in a bent state was measured. The results revealed robust device properties over a range of bending radii (R_C), as shown in figure 4(a). The bending characteristic curve plots the current hysteresis loop in the voltage range of 10 to −10 V at bending radii of ∞, 21, 14, 11, 9 mm, and the returned state, corresponding to 0, 0.06, 0.09, 0.11, 0.13% strained states and initial states, respectively. The measured current loops varied slightly with the bending radius. The currents (normalized relative to the initial on/off currents) varied within 20%, indicating that the devices were quite stable under strains of up to 0.13%. The devices were not observed to fracture during the bending test, as shown in figure 4(b) and the inset data.

4. Conclusion

In summary, this paper reports the demonstration of flexible graphene-based FeFET memory devices prepared on a plastic substrate. High quality PZT thin films were prepared using a sol–gel method and transferred to a plastic substrate. The anti-ferroelectric properties of the PZT and graphene were compensated by treating the device with an electrolyte solution. The resulting devices displayed ferroelectric memory properties and a mechanical stability on the plastic substrate. The results presented here suggest that a single transistor type in a FeFET memory device prepared from an inorganic PZT thin film could be integrated onto a flexible substrate to yield a robust device performance.

Acknowledgments

This work was supported by the Basic Research Program (2012R1A2A1A03006049 and 2009-0083540) through the National Research Foundation of Korea (NRF), funded by the Ministry of Education, Science and Technology and the Development Program of Manufacturing Technology for Flexible Electronics with High Performance (SC0970) funded by Korea Institute of Machinery and Materials (KIMM). BO acknowledges support from NUS-YIA (R144-000-283-101) and the Singapore Millennium Foundation-NUS Research Horizons Award 2009 (Nos R-144-001-271-592 and R-144-001-271-646).

References

[1] Gelinck G H *et al* 2004 Flexible active-matrix displays and shift registers based on solution-processed organic transistors *Nature Mater.* **3** 106–10
[2] Forrest S R 2004 The path to ubiquitous and low-cost organic electronic appliances on plastic *Nature* **428** 911–8
[3] Reuss R H *et al* 2005 Macroelectronics: perspectives on technology and applications *Proc. IEEE* **93** 1239–56
[4] Liao L *et al* 2009 Ferroelectric transistors with nanowire channel: toward nonvolatile memory applications *ACS Nano* **3** 700–6
[5] Fu W, Xu Z, Bai X, Gu C and Wang E 2009 Intrinsic memory function of carbon nanotube-based ferroelectric field-effect transistor *Nano Lett.* **9** 923–5
[6] Grantab R, Shenoy V B and Ruoff R S 2010 Anomalous strength characteristics of tilt grain boundaries in graphene *Science* **330** 946–8
[7] Fang F, Yang W, Zhang M J and Zhang F C 2007 Deformation and molecular chain evolution of poly(vinylidene

fluoride-trifluoroethylene) copolymer films under combined electrical and mechanical loads *J. Appl. Phys.* **101** 053531

[8] Bae S-H, kahya O, Sharma B K, Kwon J, Cho H J, Özyilmaz B and Ahn J-H 2013 Graphene-P(VDF-TrFE) multilayer film for flexible applications *ACS Nano* **7** 3130–8

[9] Ni G-X, Zheng Y, Bae S, Tan C Y, Kahya O, Wu J, Hong B H, Yao K and Özyilmaz B 2012 Graphene–ferroelectric hybrid structure for flexible transparent electrodes *ACS Nano* **6** 3935–42

[10] Doh Y-J and Yi G-C 2010 Nonvolatile memory devices based on few-layer graphene films *Nanotechnology* **21** 105204

[11] Zheng Y, Ni G-X, Toh C-T, Zeng M-G, Chen S-T, Yao K and Özyilmaz B 2009 Gate-controlled nonvolatile graphene–ferroelectric memory *Appl. Phys. Lett.* **94** 163505

[12] Zheng Y, Ni G-X, Toh C-T, Yao K and Özyilmaz B 2010 Graphene field-effect transistors with ferroelectric gating *Phys. Rev. Lett.* **105** 166602

[13] Rho J, Kim S J, Heo W, Lee N-E, Lee H-S and Ahn J-H 2010 $PbZr_xTi_{1-x}O_3$ ferroelectric thin-film capacitors for flexible nonvolatile memory applications *IEEE Electron Device Lett.* **31** 1017–9

[14] Kwon J, Seung W, Sharma B K, Kim S-W and Ahn J-H 2012 A high performance PZT ribbon-based nanogenerator using graphene transparent electrode *Energy Environ. Sci.* **5** 8970–5

[15] Hong X, Hoffman J, Posadas A, Zou K, Ahn C H and Zhu J 2010 Unusual resistance hysteresis in *n*-layer graphene field effect transistors fabricated on ferroelectric $Pb(Zr_{0.2}Ti_{0.8})O_3$ *Appl. Phys. Lett.* **97** 033114

[16] Song E B *et al* 2011 Robust bi-stable memory operation in single-layer graphene ferroelectric memory *Appl. Phys. Lett.* **99** 042109

[17] Kataoka S, Arie T and Akita S 2011 Improvement of transfer characteristic for carbon nanotube field effect transistor with poly crystalline $PbZr_xTi_{1-x}O_3$ gate by ionic liquid *Appl. Phys. Lett.* **99** 223514

[18] Lee Y H, Lee J-K and Hong K S 2003 Influence of Zr/Ti ratio and preferred orientation on polarization switching and domain configuration of $Pb(Zr_{1-x}Ti_x)O_3$ thin films *J. Korean Phys. Soc.* **42** 1395–8

[19] Gardeniers J G E, Smith A and Cobianu C 1995 Characterisation of sol–gel PZT films on Pt-coated substrates *J. Micromech. Microeng.* **5** 153–5

[20] Chen S-Y and Sun C-L 2001 Ferroelectric characteristics of oriented $Pb(Zr_{1-x}Ti_x)O_3$ films *J. Appl. Phys.* **90** 2970–4

[21] Chen S-Y and Chen I-W 1997 Comparative role of metal–organic decomposition-derived [100] and [111] in electrical properties of $Pb(Zr, Ti)O_3$ thin films *Japan. J. Appl. Phys.* **36** 4451–8

[22] Dean C R *et al* 2010 Boron nitride substrates for high-quality graphene electronics *Nature Nanotechnol.* **5** 722–6

[23] McKenna K P and Shluger A L 2008 Electron-trapping polycrystalline materials with negative electron affinity *Nature Mater.* **7** 859–62

[24] Kim W, Javey A, Vermesh O, Wang Q, Li Y and Dai H 2003 Hysteresis caused by water molecules in carbon nanotube field-effect transistors *Nano Lett.* **3** 193–8

[25] Wang S, Ang P K, Wang Z, Tang A L L, Thong J T L and Loh K P 2010 High mobility, printable, and solution-processed graphene electronics *Nano Lett.* **10** 92–8

[26] Chen F, Xia J and Tao N 2009 Ionic screening of charged-impurity scattering in graphene *Nano Lett.* **9** 1621–5

[27] Cho J H, Lee J, He Y, Kim B, Lodge T P and Frisbie C D 2008 High-capacitance ion gel gate dielectrics with faster polarization response times for organic thin film transistors *Adv. Mater.* **20** 686–90

[28] Drahushuk L W and Strano M S 2012 Mechanisms of gas permeation through single layer graphene membranes *Langmuir* **28** 16671–8

[29] Zhao Y, Xie Y, Hui Y Y, Tang L, Jie W, Jiang Y, Xu L, Lau S P and Chai Y 2013 Highly impermeable and transparent graphene as an ultra-thin protection barrier for Ag thin films *J. Mater. Chem.* C **1** 4956–61

[30] Lee M J, Choi J S, Kim J-S, Byun I-S, Lee D H, Ryu S, Lee C and Park B H 2012 Characteristics and effects of diffused water between graphene and a SiO_2 substrate *Nano Res.* **5** 710–7

[31] Kim J-S *et al* 2013 Between scylla and charybdis: hydrophobic graphene-guided water diffusion on hydrophilic substrates *Sci. Rep.* **3** 2309

[32] Kim B J, Jang H, Lee S-K, Hong B H, Ahn J-H and Cho J H 2010 High-performance flexible graphene field effect transistors with ion gel gate dielectrics *Nano Lett.* **10** 3464–6

[33] Pachoud A, Jaiswal M, Ang P K, Loh K P and Özyilmaz B 2010 Graphene transport at high carrier densities using a polymer electrolyte gate *Europhys. Lett.* **92** 27001

[34] Das A, Chakraborty B and Sood A K 2008 Raman spectroscopy of graphene on different substrates and influence of defects *Bull. Mater. Sci.* **31** 579–84

[35] Bartolomeo A D, Giubileo F, Santandrea S, Romeo F, Citro R, Schroeder T and Lupina G 2011 Charge transfer and partial pinning at the contacts as the origin of a double dip in the transfer characteristics of graphene-based field-effect transistors *Nanotechnology* 275702

[36] Das A *et al* 2008 Monitoring dopants by Raman scattering in an electrochemically top-gated graphene transistor *Nature Nanotechnol.* **3** 210–5

[37] Zheng Y *et al* 2011 Wafer-scale graphene/ferroelectric hybrid devices for low-voltage electronics *Europhys. Lett.* **93** 17002

[38] Meneghini M, Trevisanello L-R, Zehnder U, Zahner T, Strauss U, Meneghesso G and Zanoni E 2006 High-temperature degradation of GaN LEDs related to passivation *IEEE Trans. Electron Devices* **53** 2981–7

[39] Miura K and Tanaka M 1996 Origin of fatigue in ferroelectric perovskite oxides *Japan. J. Appl. Phys.* **35** 2719–25